J. Fluid Mech. (1983), *vol.* 137, *pp.* 423–445
Printed in Great Britain

Three-dimensional baroclinic instability of a Hadley cell for small Richardson number

By BASIL N. ANTAR
The University of Tennessee Space Institute, Tullahoma, TN 37388

AND WILLIAM W. FOWLIS
Space Science Laboratory, NASA Marshall Space Flight Center, Huntsville, AL 35812

(Received 14 January 1983 and in revised form 29 August 1983)

A three-dimensional linear stability analysis of a baroclinic flow for Richardson number Ri of order unity is presented. The model considered is a thin, horizontal, rotating fluid layer which is subjected to horizontal and vertical temperature gradients. The basic state is a Hadley cell which is a solution of the Navier–Stokes and energy equations and contains both Ekman and thermal boundary layers adjacent to the rigid boundaries; it is given in closed form. The stability analysis is also based on the Navier–Stokes and energy equations; and perturbations possessing zonal, meridional and vertical structures were considered. Numerical methods were developed for the solution of the stability problem, which results in an ordinary differential eigenvalue problem. The objectives of this work were to extend the previous theoretical work on three-dimensional baroclinic instability for small Ri to a more realistic model involving the Prandtl number σ and the Ekman number E, and to finite growth rates and a wider range of the zonal wavenumber. The study covers ranges of $0.135 \leqslant Ri \leqslant 1.1$, $0.2 \leqslant \sigma \leqslant 5.0$, and $2 \times 10^{-4} \leqslant E \leqslant 2 \times 10^{-3}$. For the cases computed for $E = 10^{-3}$ and $\sigma \neq 1$, we found that conventional baroclinic instability dominates for $Ri > 0.825$ and symmetric baroclinic instability dominates for $Ri < 0.675$. However, for $E \geqslant 5 \times 10^{-4}$ and $\sigma = 1$ in the range $0.3 \leqslant Ri \leqslant 0.8$, conventional baroclinic instability always dominates. Further, we found in general that the symmetric modes of maximum growth are not purely symmetric but have weak zonal structure. This means that the wavefronts are inclined at a small angle to the zonal direction. The results also show that as E decreases the zonal structure of the symmetric modes of maximum growth rate also decreases. We found that when zonal structure is permitted the critical Richardson number for marginal stability is increased, but by only a small amount above the value for pure symmetric instability. Because these modes do not substantially alter the results for pure symmetric baroclinic instability and because their zonal structure is weak, it is unlikely that they represent a new type of instability.

1. Introduction

Stably stratified baroclinic flow can be destabilized by several different mechanisms. The most extensively studied of these instabilities is usually referred to simply as baroclinic instability. For this type of instability the Richardson number Ri is much greater than unity, and the quasigeostrophic equations (Pedlosky 1979) are valid. The perturbations of maximum growth rate have a wavelength in the zonal

(azimuthal) direction, and, in the absence of horizontal shear, the gravest possible structure in the meridional direction (Charney 1947; Eady 1949). This instability has been observed in the laboratory, and is the cause of mid-latitude wave cyclones (Lorenz 1967; Hide & Mason 1975).

A second type of instability, known as symmetric baroclinic instability, occurs for Ri of order unity, and requires a more general set of equations than the quasigeostrophic set. In this case, the perturbations of maximum growth rate have meridional structure but no, or only weak, zonal structure. The study presented in this paper is concerned with this type of instability. Since this instability occurs in only a small range of Ri, there would appear to be few geophysical applications. However, Stone (1967) conjectured that the banded structure of Jupiter's atmosphere is caused by this instability, and Bennets & Hoskins (1979) and Emanuel (1979) suggested that rain bands and squall lines may be due to this instability. Two of the earliest analyses of symmetric baroclinic instability are those of Solberg (1936) and Kuo (1956). In these papers purely two-dimensional perturbations with no zonal structure were considered.

Stone (1966, 1970, 1971) was the first to examine the stability of baroclinic flow for small Ri with respect to three-dimensional perturbations. For the basic state Stone took a plane parallel baroclinic flow with constant temperature gradients and a constant vertical shear consistent with the thermal wind balance. Horizontal shear was excluded. Viscous and thermal diffusion effects were neglected in both the basic state and perturbation analyses. In this paper such a basic state will be referred to as the Eady basic state. Stone found that conventional baroclinic instability dominates if $Ri \geqslant 0.95$, symmetric baroclinic instability dominates if $0.25 \leqslant Ri \leqslant 0.95$, and Kelvin–Helmholtz instability dominates if $Ri \leqslant 0.25$. For symmetric instability, Stone found that the wavelength of maximum growth rate is zero. It cannot be concluded with reasonable certainty that symmetric baroclinic instability has been observed in the laboratory. Stone's results motivated a laboratory search, and some evidence of the predicted meridional structure was observed (Stone *et al.* 1969; Hadlock, Na & Stone 1972). However, Stone's theoretical model was somewhat different from the experimental realization and conclusive results were not obtained. Calman (1977) attributed certain experimental observations to symmetric baroclinic instability. However, there were large discrepancies with the theory.

In the theoretical studies on symmetric baroclinic instability which followed Stone's analyses, workers added viscous and thermal effects to make the models more realistic. However, in all but one of these studies (Busse & Chen 1981; see below), attention was restricted to two-dimensional perturbations with no zonal structure. McIntyre (1970) considered an Eady basic state with viscosity and thermal diffusivity included in the perturbation analysis. He chose an unbounded model. McIntyre found, in the absence of horizontal shear, that, for the Prandtl number σ equal to unity, the critical Richardson number Ri_c is also equal to unity, and, for $\sigma \neq 1$, Ri_c increases above unity. These results are shown in figure 1 (*a*). Thus double-diffusive effects further destabilize the flow. McIntyre's choice of a lengthscale and unbounded model were such that the Ekman number E disappears formally from his problem. Emanuel (1979) considered the same model as McIntyre but for a vertically bounded flow. Emanuel studied (i) hydrostatic disturbances and (ii) non-hydrostatic disturbances in a neutrally stratified fluid. He investigated only neutral modes by invoking the principle of exchange of stabilities. For both of the above cases Emanuel found that Ri_c depends on both σ and E. He also established that the wavelength of the

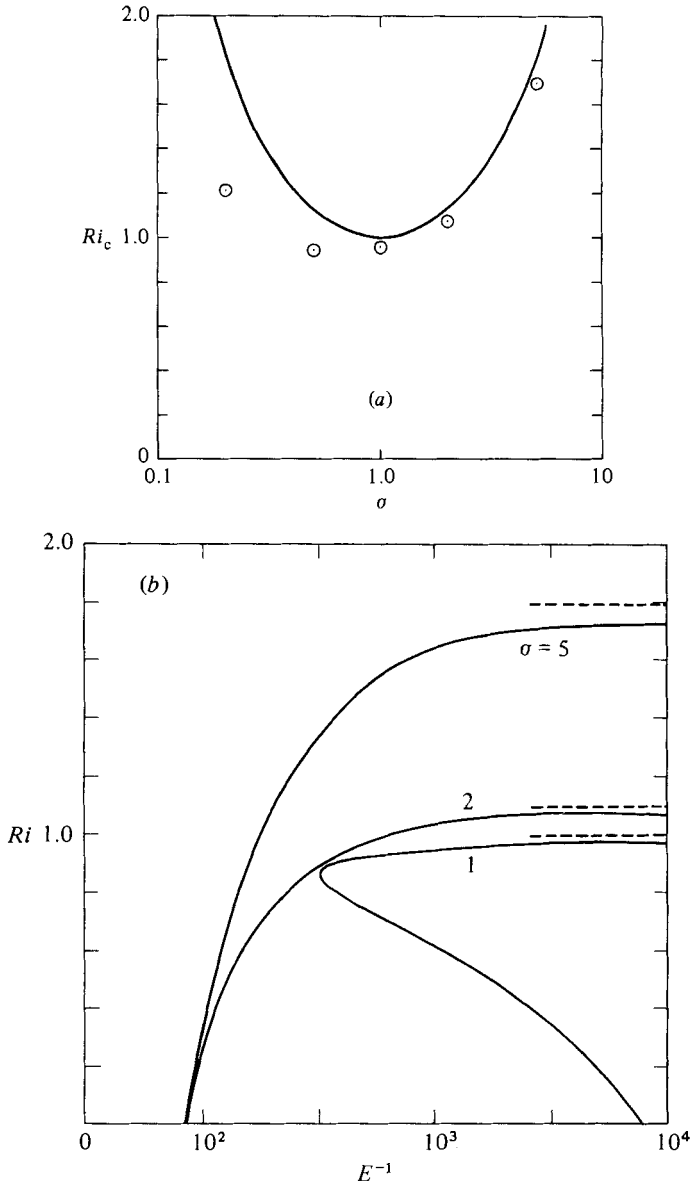

FIGURE 1. (*a*) The critical Richardson number as a function of the Prandtl number: —— according to McIntyre (1970); ⊙, according to Antar & Fowlis (1982). (*b*) Marginal stability curves as functions of E and Ri for three values of σ and for $l = 4$. The dashed curves are McIntyre's results.

most-unstable normal mode is determined primarily by the depth of the fluid and the slopes of the isentropic surfaces rather than by the diffusive properties of the fluid.

In all of the theoretical studies cited above, the Eady basic state was used. In an experimental apparatus whose upper and lower boundaries are stationary, such a basic state is a good approximation in the interior of the fluid only; it is not a good approximation near the boundaries especially when E is not vanishingly small. Antar & Fowlis (1982; hereinafter referred to as AF) presented a two-dimensional theoretical study of symmetric baroclinic instability for a fluid contained between two horizontal

plates of infinite extent. The analysis used a realistic basic state which was obtained as an analytical solution of the Navier–Stokes and energy equations. This solution included both the Ekman and thermal layers adjacent to the boundaries. The stability analysis also included viscous and thermal diffusion effects and was performed numerically. AF found that the instability sets in when Ri is close to unity and that Ri is a strong function of both σ and E. Figure 1 (a) shows these results for Ri_c as a function of σ for fixed E and compares their results with those found by McIntyre (1970). For fixed σ, AF found that Ri_c decreases with increasing E until a critical value of E is reached beyond which the flow is stable. These results are shown in figure 1 (b). The analysis was not restricted to critical values, and the influence of σ and E on the growth rate was also determined. For the range of parameter values considered, the most unstable wavelength was about half the depth. The nonlinear basic state was also used by Antar & Fowlis (1981) in a study of the conventional baroclinic instability. More exhaustive discussions of the previous theoretical work dealing with two-dimensional studies of symmetric baroclinic instability have been given by Emanuel (1979) and AF.

Recently Busse & Chen (1981) extended Stone's studies by including thermal and viscous diffusion effects in a three-dimensional analysis of symmetric baroclinic instability. The basic state was an Eady basic state in which the horizontal boundaries moved consistently with the thermal wind to eliminate Ekman layers on the boundaries. Busse & Chen confined their analysis to critical values, and they obtained their solution through an expansion in the zonal wavenumber k. Thus their solution is restricted to small k. They showed, in the limit of small E, that the mode of symmetric instability at maximum Ri_c exhibits an angle of inclination with the direction of the basic state flow. And they showed further that the sign of the angle depends upon whether $\sigma \lessgtr 1$. They also showed that the range of Ri for which the instability occurs is increased beyond the limits of the two-dimensional problem solved by McIntyre (1970).

The objectives of the present study were to extend the previous work on three-dimensional baroclinic instability for $Ri = O(1)$. The work of Stone (1966, 1970, 1971) is extended to a more realistic model involving viscous and thermal dissipation and the work of Busse & Chen (1981) to finite growth rates and a wider range of the zonal wavenumber. The basic state chosen was that used previously by Antar & Fowlis (1981) and AF. The stability analysis was performed through numerical integration of the perturbation equations. Critical values and growth rates are presented.

In §2 the equations and solution of the basic state are presented. Also in §2 the equations and method of solution for the stability analysis are described. In §3 the results of the stability analysis are presented and discussed. The main results are summarized in §4.

2. The equations and their solution

2.1. *The basic state*

We consider a Boussinesq fluid confined between two horizontal plates which are set a distance d apart. The coordinate system used is rectangular Cartesian with axes (x, y, z) corresponding to the eastward, northward, and vertical directions respectively, with the origin set at mid-depth between the plates. The plates and the fluid are assumed to extend to infinity in the x- and y-directions. Also, the plates and the fluid are taken to rotate as a whole about the vertical axis with a constant angular velocity,

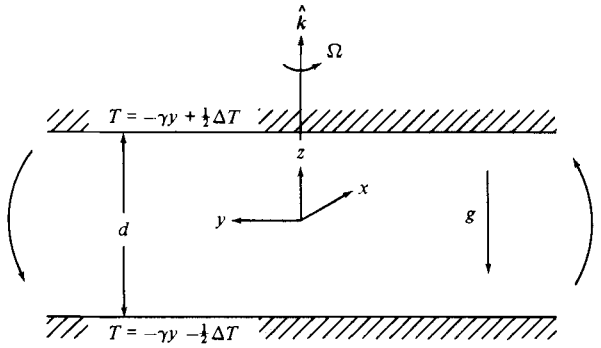

FIGURE 2. A sketch of the model.

Ω. To maintain baroclinicity, a temperature distribution is imposed on both plates in which the temperature is made to decrease in the y-direction. Also, to ensure that the vertical stratification, and hence the Richardson number, can be arbitrarily and externally adjusted, the temperature of both the upper and lower plates are set to differ uniformly by a constant amount ΔT for all y. A sketch of the model considered is shown in figure 2.

The basic-state velocity and temperature fields are governed by the Navier–Stokes, energy and mass-conservation equations. Centrifugal effects are neglected. These equations, in dimensionless form, for the configuration described above, and for a two-dimensional steady state in a rotating reference frame, can be reduced to the following:

$$-2V = E\frac{\partial^2 U}{\partial z^2}, \tag{2.1}$$

$$2U = E\frac{\partial^2 V}{\partial z^2} - \frac{\partial p}{\partial y}, \tag{2.2}$$

$$V\frac{\partial T}{\partial y} = \frac{E}{\sigma\epsilon}\frac{\partial^2 T}{\partial z^2}, \tag{2.3}$$

$$T = \frac{\partial p}{\partial z}, \tag{2.4}$$

where $\boldsymbol{V} = (U, V)$ is the velocity vector, p the pressure, T the temperature and

$$\epsilon = \frac{\alpha g \gamma}{\Omega^2}, \quad E = \frac{\nu}{\Omega d^2}, \quad \sigma = \frac{\nu}{\kappa}$$

are a thermal Rossby number, the Ekman number, and the Prandtl number respectively. In (2.1)–(2.4), length, time, velocity and temperature were made dimensionless using d, Ω^{-1}, $\alpha g d\gamma/\Omega$ and γd respectively. α is the coefficient of thermal expansion, γ is the imposed horizontal boundary temperature gradient, and g is the acceleration due to gravity. A further assumption used in deriving (2.1)–(2.4) is that, throughout the region of interest in the fluid, the vertical velocity component W is negligible.

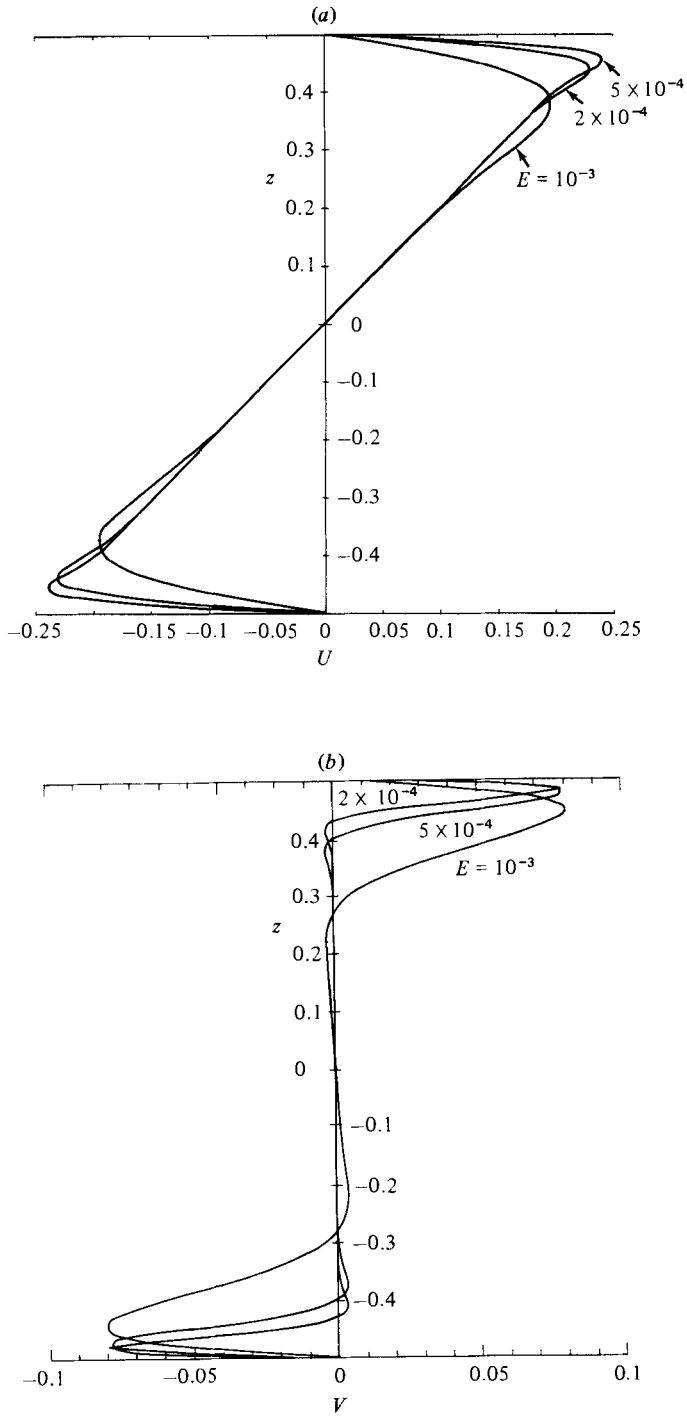

FIGURE 3(*a*, *b*). For caption see facing page.

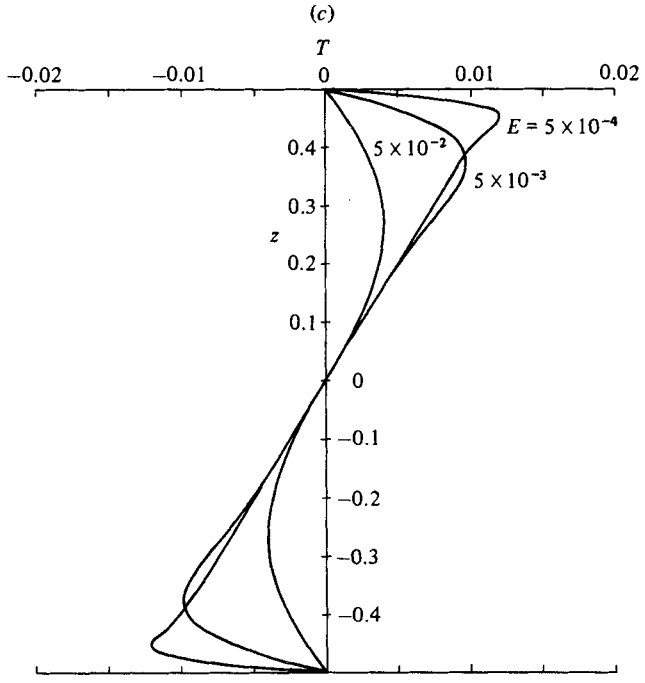

FIGURE 3. (*a*) The basic-state zonal velocity profile as a function of height according to (2.6) for three values of the Ekman number. (*b*) The meridional velocity profile. (*c*) The temperature profile for $y = 0$, $\sigma = 1$, $\epsilon = 1$ and $\Delta T = 0$.

The solution to (2.1)–(2.4) that is consistent with the no-slip and the perfectly conducting boundary conditions at the solid boundaries, i.e.

$$U = V = 0, \quad T = \pm\tfrac{1}{2}\Delta T - y \quad (z = \pm\tfrac{1}{2}), \tag{2.5}$$

is given by

$$U(z) = -\tfrac{1}{8}f(z) + \tfrac{1}{2}z, \tag{2.6a}$$

$$V(z) = -\tfrac{1}{8}g(z), \tag{2.6b}$$

$$T(y, z) = -y + (\Delta T + \tfrac{1}{4}\sigma\epsilon)\, z - \tfrac{1}{16}\sigma\epsilon f(z), \tag{2.6c}$$

where

$$f(z) = [\cosh R(z+\tfrac{1}{2}) \cos R(z-\tfrac{1}{2}) - \cosh R(z-\tfrac{1}{2}) \cos R(z+\tfrac{1}{2})]/h(R),$$

$$g(z) = [\sinh R(z+\tfrac{1}{2}) \sin R(z-\tfrac{1}{2}) - \sinh R(z-\tfrac{1}{2}) \sin R(z+\tfrac{1}{2})]/h(R),$$

$$h(R) = \sinh^2 \tfrac{1}{2}R + \sin^2 \tfrac{1}{2}R,$$

$$R = E^{-\frac{1}{4}}.$$

An assumption made in obtaining the above solutions is that the dimensionless horizontal temperature gradient $\partial T/\partial y$ is constant and equal to -1 throughout the fluid. The assumptions and limitations of this model are discussed more fully in Antar & Fowlis (1981).

The velocity and temperature profiles given by expressions (2.6) are shown in figure 3 for representative values of E, ϵ, σ and ΔT.

2.2. *The perturbation equations*

To study the stability of the stationary basic state, the dependent variables (velocity, temperature and pressure) are first decomposed into basic-state and perturbation

components. The equations governing the perturbation components are obtained by substituting the variables into the Navier–Stokes and energy equations, subtracting the basic state, and linearizing. Since the resulting equations are linear, with coefficients depending on z alone, they admit of separable solutions of the form

$$[u', v', w', \theta', p'] = [u(z), v(z), \theta(z), p(z)] \exp[\mathrm{i}(kx + ly - \omega t)],$$

where $\boldsymbol{u}'(u', v', w')$, p' and θ' are the perturbation velocity vector, pressure, and temperature respectively.

This solution represents a travelling oblique wave with frequency ω and wavenumber components k and l in the zonal and the meridional directions respectively. After substituting the above solution into the governing perturbation equations and eliminating the pressure, the linearized momentum and energy equations can be written as

$$\mathrm{i}[\omega - \epsilon(kU + lV)]\nabla^2 w + \mathrm{i}\epsilon(k\,\mathrm{D}^2 V + l\,\mathrm{D}^2 U)\,w - 2\mathrm{i}(k\,\mathrm{D}v - l\,\mathrm{D}u) = -E\nabla^2\nabla^2 w + m^2\theta, \tag{2.7}$$

$$\mathrm{i}[\omega - \epsilon(kU + lV)][m^2 v - \mathrm{i}l\,\mathrm{D}w] - \epsilon k w(k\,\mathrm{D}V - l\,\mathrm{D}U) - 2\mathrm{i}k\,\mathrm{D}w = -E\nabla^2(m^2 v - \mathrm{i}l\,\mathrm{D}w), \tag{2.8}$$

$$\mathrm{i}\sigma[\omega - \epsilon(kU + lV)]\theta + \epsilon\sigma(v - w\,\mathrm{D}T) = -E\nabla^2\theta, \tag{2.9}$$

where

$$\mathrm{D}w + \mathrm{i}ku + \mathrm{i}lv = 0,$$

$$\nabla^2 = \mathrm{D}^2 - m^2,$$

$$m^2 = k^2 + l^2,$$

and $\mathrm{D} = \mathrm{d}/\mathrm{d}z$ is a differential operator. In the above U, V and T are the basic-state velocity and temperature fields, which are non-simple functions of z. The perturbation velocity and temperature vanish on the plates, implying that

$$w = \mathrm{D}w = v = \theta = 0 \quad (z = \pm\tfrac{1}{2}). \tag{2.10}$$

The problem defined by (2.7)–(2.9) with the boundary conditions (2.10) defines an eigenvalue problem of the form

$$\mathscr{F}(E, \epsilon, \sigma, \Delta T, k, l, \omega) = 0, \tag{2.11}$$

where the frequency ω is in general complex for the temporal stability problem. The basic state is stable or unstable depending on whether $\mathrm{Im}(\omega) = \omega_\mathrm{i} < 0$ or $\omega_\mathrm{i} > 0$ respectively. For marginal stability for which $\omega_\mathrm{i} = 0$, $\mathrm{Re}(\omega) = \omega_\mathrm{r}$, and either E or ϵ are chosen as the eigenvalues. In most of the results described in §3, the growth rate ω_i, was used as a function of any of the parameters to determine the most unstable mode.

As indicated in §1, previous studies of symmetric baroclinic instability have selected the Richardson number as a parameter. However, owing to the specific non-dimensionalization chosen for this study, Ri does not appear as an explicit parameter in (2.11). Ri is defined as the ratio of the vertical stratification to the square of the shear, i.e.

$$Ri = \alpha g \frac{\partial T^*}{\partial z^*} \Big/ \left(\frac{\partial U^*}{\partial z^*}\right)^2, \tag{2.12}$$

where the asterisk denotes a dimensional quantity. Since in the present problem this definition implies a variable Ri as a function of height, a more convenient definition of Ri is its value at mid-depth in the channel. Substituting the values of the

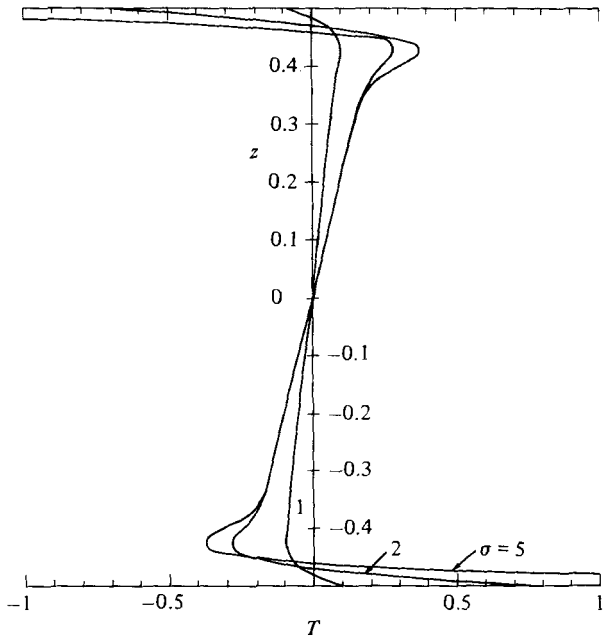

FIGURE 4. The temperature profile for $E = 10^{-3}$ and three values of the Prandtl number: $\sigma = 1$, $\Delta T = -0.2$, $\epsilon = 1.6$; $\sigma = 2$, $\Delta T = -1.5$, $\epsilon = 4.0$; $\sigma = 5$, $\Delta T = -4.5$, $\epsilon = 4.0$.

temperature and velocity gradients of the basic state (expressions (2.6)) at $z = 0$ into the above definition, we obtain

$$Ri_0 = 4\epsilon^{-1}(\Delta T + \tfrac{1}{4}\sigma\epsilon) + O(Re^{-\frac{1}{2}R}), \tag{2.13}$$

which is a constant defined exclusively by the basic state. Note that for $E < 10^{-2}$ (i.e. $R > 10$), which is the range of E for all the calculations presented in §3, the last term in (2.13) is negligible. Since Ri_0 is a complicated function of the basic state, care is required in selecting values of the basic state parameters to achieve desired values of Ri_0. (From this point on we shall drop the suffix from Ri_0.) Examination of (2.13) reveals that, to obtain values of Ri close to unity, ΔT must be greater or less than zero depending on whether $\sigma < 1$ or $\sigma > 1$ respectively. Note that for some values of $\Delta T < 0$ there does exist a large region in the interior of the fluid with stable stratification. This is shown in figure 4, which is based on parameter values for the computations whose results are discussed in §3. This problem of the selection of the basic-state parameters to achieve specific values of Ri is discussed more fully in AF.

Note that setting $k = 0$ in the perturbation equations allows for only axisymmetric waves propagating in the meridional direction, and setting $l = 0$ allows for only waves propagating in the zonal direction.

2.3. *Method of solution*

The governing differential equations (2.7)–(2.9) with boundary conditions (2.10) form an eigenvalue problem for which a non-trivial solution should be available. Owing to the complexity of the coefficients of these equations (a consequence of the non-simple basic state), a closed-form solution cannot be found. The only way to solve this problem for the ranges of all the parameters involved is by numerical means. There are basically two direct methods for the numerical solution of differential eigenvalue problems. These are the matrix and the shooting methods. Owing to the complexity

of our system (viz a system of coupled, eight ordinary differential equations), the shooting technique is the most straightforward to implement. For small values of the Ekman number, the shooting procedure can be successful only if it is used in conjunction with a filtering or orthonormalization scheme (see e.g. Conte 1966). Otherwise the inevitable presence of the rapidly growing solution of the differential system can quickly render the linearly independent solution numerically dependent.

For the solution of the present eigenvalue problem, a computer code was developed with an eighth-order variable-step Runge–Kutta–Fehlberg initial-value integrator. For the iteration procedure a Newton–Raphson method was used, and the orthonormalization process was implemented at each integration step. All of the eigenvalues that are presented in §3 were produced with a relative tolerance of 10^{-4} in the iteration process (i.e. all of the eigenvalues presented are correct up to four significant figures). For small enough Ekman numbers, the Ekman and the thermal layers along the plates are very thin, and the code was made to take at least 10 steps within each layer to assure adequate representation of these layers. Normally this method requires an initial guess for the eigenvalue, and the whole process for obtaining the results is started by first trying several guesses. Once a convergence on an eigenvalue was obtained, that eigenvalue was used as the initial estimate for obtaining a neighbouring one, and the process was repeated. Typically, if an eigenvalue existed, convergence was achieved in under 10 iterations.

3. Results and discussion

In this section we present the results of a three-dimensional study of baroclinic instability for $Ri = O(1)$. All of the results were obtained using the basic state defined by (2.6) and by means of the solution of the eigenvalue problem described by (2.7)–(2.10) and represented functionally by (2.11). We begin by presenting plots of the growth rate ω_i, as a function of the zonal wavenumber k for selected values of the meridional wavenumber l for a range of values of Ri and for fixed values of σ, ΔT and E. The values of ΔT were selected so that $Ri = O(1)$ (see §2). For fixed values of σ, ΔT and E, Ri was varied by varying ϵ. We continue by presenting plots of the growth rate maxima $\omega_i(\max)$, and the corresponding $k(\max)$, as functions of Ri for selected values of l and for a range of values of σ. The actual values of σ chosen are in the range $0.2 \leqslant \sigma \leqslant 5.0$, which includes real liquids. For all the above results $E = 10^{-3}$. Next we present plots of ω_i versus k for selected values of l, for fixed values of Ri and σ and for a range of values of E. The values of E chosen are in the range $2 \times 10^{-4} \leqslant E \leqslant 2 \times 10^{-3}$. The previous work on two-dimensional instability (AF) showed that, for the smaller values of E in this range, Ri_c is close to its asymptotic limit. The use of still smaller values of E would have substantially increased the computing time (see §2). The range of values of E is realistic for typical laboratory apparatus and liquids.

Figures 5–7 show ω_i versus k for three values of Ri, $\sigma = 2$, $E = 10^{-3}$, and $\Delta T = -1.5$. Figure 5 for $Ri = 0.93$ shows that pure symmetric waves ($k = 0$) do grow and that their growth rates increase with increasing l reaching a maximum at about $l = 8$ and then decrease for a further increase in l. However, the overall maximum growth rate is associated with the conventional baroclinic instability mechanism ($l = 0$). The mode ($k = 0.88$, $l = 0$) has the maximum growth rate. Figure 6 shows that, for $Ri = 0.80$, the growth rates for the symmetric modes have increased substantially and are comparable to the growth rates of the purely zonal waves

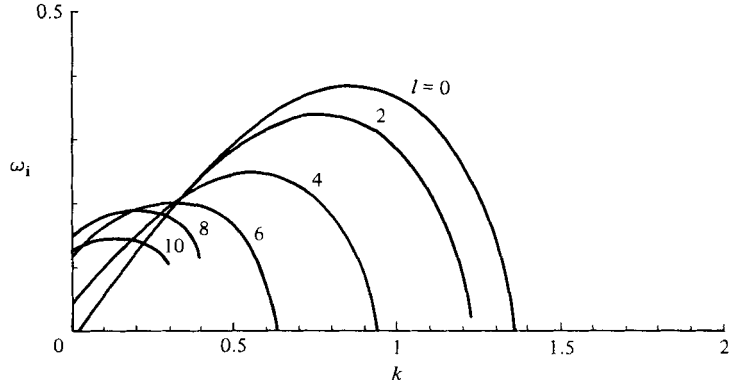

FIGURE 5. The growth rates as a function of k for $Ri = 0.93$, $\epsilon = 5.6$, $\sigma = 2$, $\Delta T = -1.5$, $E = 10^{-3}$ and selected values of l.

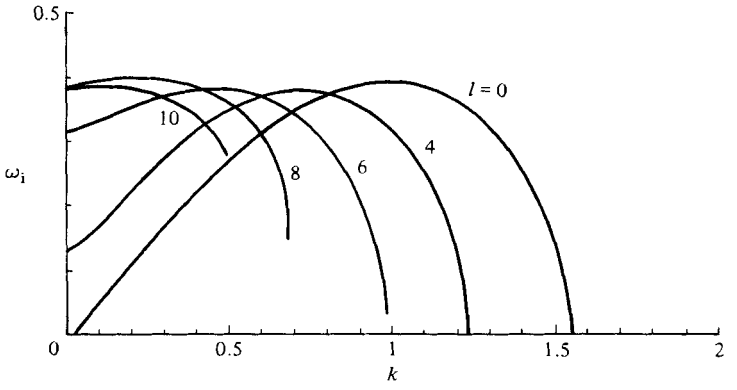

FIGURE 6. The growth rates as a function of k for $Ri = 0.80$, $\epsilon = 5.0$, $\sigma = 2$, $\Delta T = -1.5$, $E = 10^{-3}$ and selected values of l.

($l = 0$). The maximum value of ω_i shown in the figure is $\omega_i = 0.399$ for $k = 0.25$, $l = 8$, which is to be compared with $\omega_i = 0.394$ for $k = 1.0$ and $l = 0$.

In figure 6 we have shown only the curves for l up to $l = 10$. This is because we know, for the parameter values of figure 6, that the maximum value of ω_i for the pure symmetric modes occurs at $l = 8.8$. This result is shown in figure 8. The values of ω_i decrease further as l increases beyond 10, making additional curves unnecessary. As we pointed out above, for $Ri = 0.80$ the maximum growth rates of the symmetric and conventional baroclinic modes are about the same. Stone (1970) found for his inviscid model that the maximum growth rates are equal for $Ri = 0.95$. For all of the unstable modes examined in this study it was found that the propagation speed is equal to the basic-state mid-depth speed, namely $U = 0$ (i.e., for all $\omega_i > 0$, $\omega_r = 0$).

Note in figure 6 that the growth-rate maximum does not occur for a pure symmetric wave; k at the maximum value is small but not zero. An analogous result was found earlier by Busse & Chen (1981) for the waves at marginal stability (see §1). To avoid confusion in the discussion to follow, we define symmetric instability to include unstable modes for which k is small as well as zero. Further, for simplicity we shall refer to conventional baroclinic instability ($l = 0$) as zonal instability. In addition the term preferred mode will be used to mean the mode of maximum growth rate.

Figure 7 for $Ri = 0.50$ shows the effect on ω_i of a further decrease in Ri. The growth rates for the symmetric modes have continued to increase and are now considerably

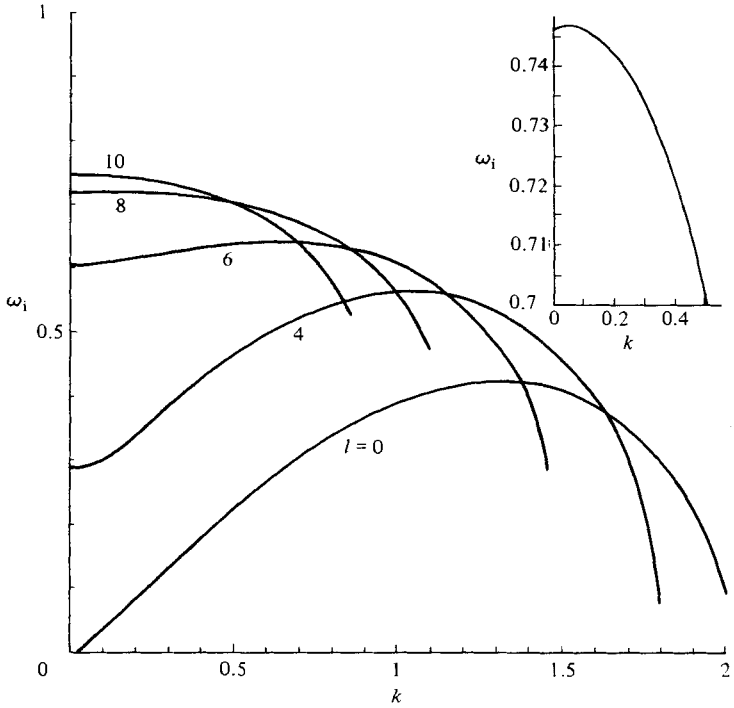

FIGURE 7. The growth rates as a function of k for $Ri = 0.5$, $\epsilon = 4.0$, $\sigma = 2$, $\Delta T = -1.5$, $E = 10^{-3}$ and selected values of l. Inset shows growth rate for $l = 10$.

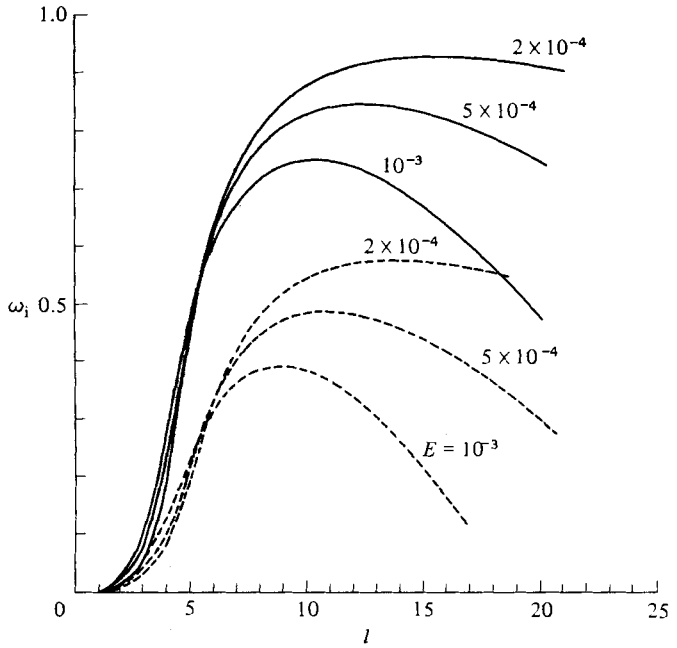

FIGURE 8. The growth rates as a function of l at $k = 0$ for $\sigma = 2.0$, $\Delta T = -1.5$, and three values of E: ——, $Ri = 0.5$; - - - -, $Ri = 0.8$.

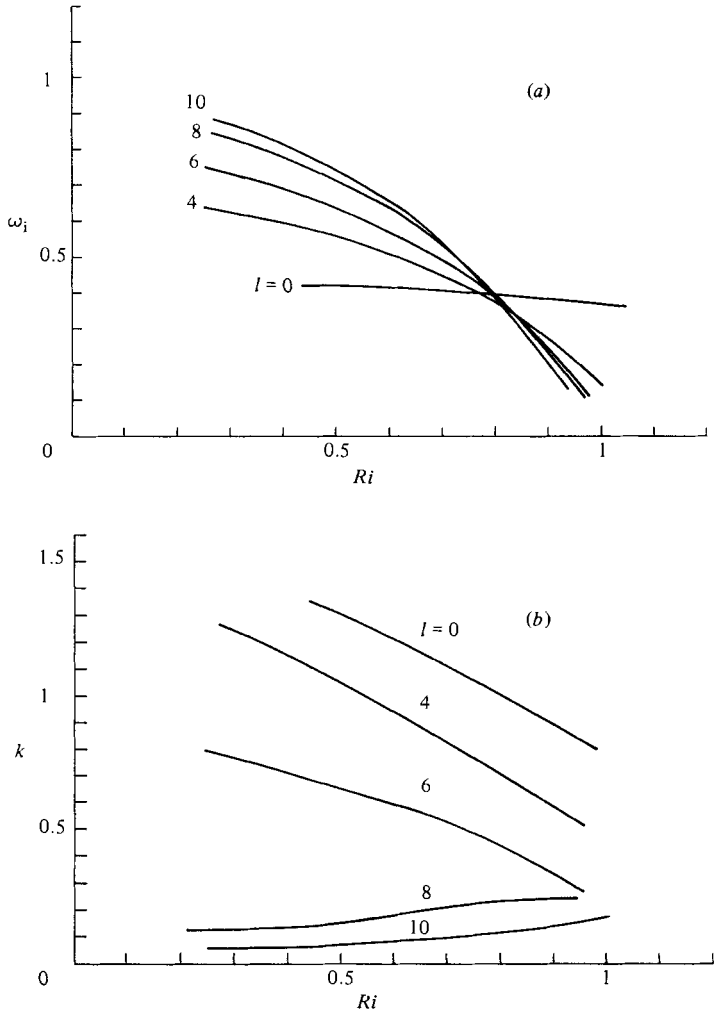

FIGURE 9. (*a*) The maximum values of ω_i as a function of Ri for $\sigma = 2.0$, $\Delta T = -1.5$, $E = 10^{-3}$ and several values of l. (*b*) The values of k at maximum ω_i as a function of Ri for the conditions of (*a*).

greater than those for the pure zonal modes. In this figure we have shown only the curves for l up to $l = 10$. Again this is because we know, for the values of the parameters of this figure, that the maximum of ω_i for the pure symmetric modes occurs at $l = 10.2$. This result is shown in figure 8. For the data in figure 7 the maximum growth rate occurs for $k \approx 0.05$ and $l = 10$. Note again that the maximum does not occur for $k = 0$. This is clearly shown in the inset in figure 7, which is a replot of the growth rate for the $l = 10$ wave with a stretched ordinate. This means that the preferred mode of symmetric baroclinic instability exhibits a slight angle of inclination with the direction of the basic state flow. This angle is given approximately by k/l.

A further reduction in Ri, for this set of parameters, leads to an increase in ω_i, for both k and l, but the overall functional dependence of ω_i on k and l remains essentially the same as the results for $Ri = 0.5$. This result is shown in figure 9(*a*), which is a plot of the growth rate maxima $\omega_i(\max)$ versus Ri for the case $\sigma = 2.0$, $\Delta T = -1.5$, $E = 10^{-3}$ and for several values of l. This figure summarizes the relevant results from

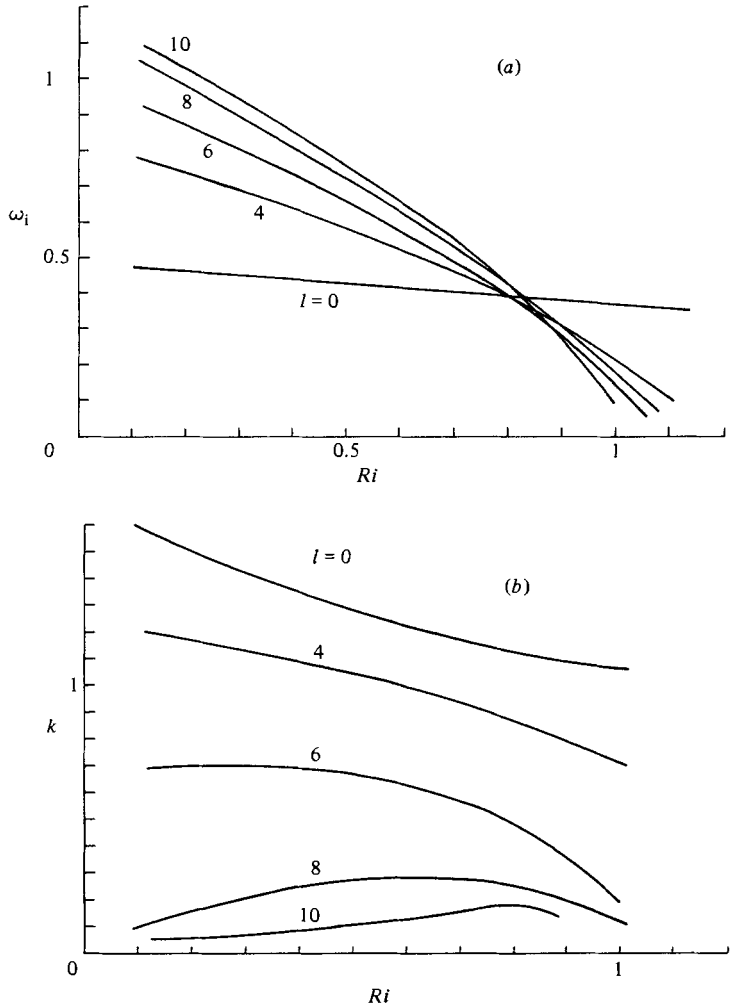

FIGURE 10. (*a*) The maximum values of ω_i as a function of Ri for $\sigma = 5.0$, $\Delta T = -4.5$, $E = 10^{-3}$ and several values of l. (*b*) The values of k at maximum ω_i as a function of Ri for the conditions of (*a*).

figures 5–7. The general trend is for $\omega_i(\max)$ to increase with decreasing Ri for all the symmetric modes ($l \neq 0$). However, $\omega_i(\max)$ for the zonal mode is not much affected by the reduction in Ri. Figure 9(*a*) also shows the value of Ri at which the symmetric modes first become dominant, Ri_t. Ri_t is defined as the largest value of Ri at which any curve for which $l \neq 0$ intersects the $l = 0$ curve. Figure 9(*b*) is a plot of the zonal wavenumber $k(\max)$ corresponding to ω_i versus Ri for the same case as figure 9(*a*). Note that the value of $k(\max)$ corresponding to the largest $\omega_i(\max)$ curve (the $l = 10$ curve) decreases slowly with decreasing Ri, but does not become zero for small Ri. This means that the dominant symmetric modes possess zonal structure which is only weakly dependent on Ri.

We now present results for another value of σ. Figures 10(*a*, *b*) summarize the behaviour of ω_i and k as functions of Ri for $\sigma = 5.0$, $\Delta T = -4.5$ and $E = 10^{-3}$. Figure 10(*a*) shows $\omega_i(\max)$ versus Ri for several values of l. The curves show the same general trends as those in figure 9(*a*). In the range $Ri < Ri_t$ for which the symmetric

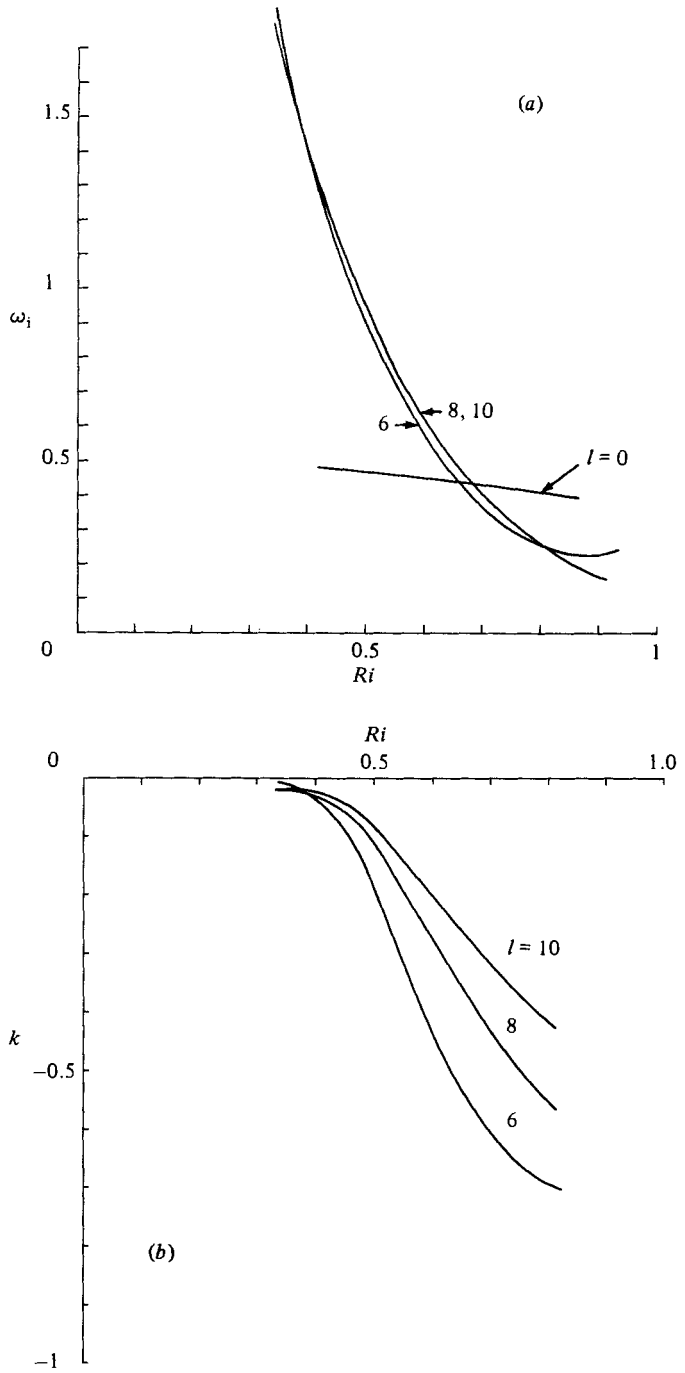

FIGURE 11. (*a*) The maximum values of ω_i as a function of Ri for $\sigma = 0.2$, $\Delta T = 0.5$, $E = 10^{-3}$ and several values of l. (*b*) The values of k at maximum ω_i as a function of Ri for the conditions of (*a*).

modes are dominant, figure 10(*a*) shows that the shortest meridional waves possess the largest values of $\omega_i(\max)$. However, we know, from computations whose results are not given here, that, for still larger values of l, $\omega_i(\max)$ decreases. The maximum of $\omega_i(\max)$ occurs for $l \approx 10$, and this l is a weak function of Ri. For the case presented

σ	Ri_t	ΔT	E
5.0	0.825	−4.5	10^{-3}
2.0	0.80	−1.5	10^{-3}
0.5	0.70	0.2	10^{-3}
0.2	0.676	0.5	10^{-3}

TABLE 1. The values of Ri_t as a function of the Prandtl number

in figure 10 $Ri_t \approx 0.825$, which is slightly larger than the value for $\sigma = 2.0$ (see figure 9*a*). Figure 10(*b*) shows k(max) versus Ri. Again it is clear that the preferred symmetric modes possess some zonal structure which for small Ri is only weakly dependent on Ri. We conclude from figures 9 and 10, for $\sigma > 1$ and in the range of σ examined, that there are no rapid changes in the character of the preferred modes as a function of Ri. Ri_t is apparently a weak function of σ.

Stone (1966, 1970) found for his non-geostrophic non-dissipative model that the preferred mode of instability changes at $Ri = 0.25$ from symmetric instability to Kelvin–Helmholtz instability (see §1). For the parameters of figure 10 we conducted growth-rate calculations for $Ri = 0.135$. The results of these calculations are included in figure 10, and they show that symmetric instability is preferred. In considering this apparent discrepancy it should be noted that Stone's conclusion was based on growth-rate behaviour for asymptotically large k; and, since growth rates for large k for our model were not computed, we cannot say anything definitive about such a transition for our model. However, for non-hydrostatic and non-dissipative models both Tokioka (1970) and Stone (1971) found that this transition did not occur. Thus it seems most probable that for our non-hydrostatic and dissipative model the transition is still less likely to occur. The earlier investigation of our model for pure symmetric modes (AF) revealed that the growth rates for these modes continues to increase as Ri is decreased through zero.

We now present results for $\sigma < 1$. Figure 11 (*a*) shows the variation of ω_i(max) with Ri for several values of l and for $\sigma = 0.2$, $\Delta T = 0.5$ and $E = 10^{-3}$. Again the symmetric modes are dominant in a range of $Ri < Ri_t$, but there are some substantial differences between this case and the results for $\sigma > 1$. The values of ω_i(max) increase more rapidly with decreasing Ri and there is not much difference among the curves for $l = 6$, 8 and 10, especially for small Ri. However, like the results for $\sigma > 1$, the curve for the zonal mode is only weakly dependent on Ri. For this case $Ri_t \approx 0.675$. From further calculations, which are not shown here, we found that, for $\sigma = 0.5$, $\Delta T = 0.2$ and $E = 10^{-3}$, $Ri_t \approx 0.7$. The values of Ri_t for all of the cases calculated are shown in table 1. Figure 11 (*b*) shows the variation of k(max) with Ri for several values of l. In this case we see a difference from the results for $\sigma > 1$; the values of k(max) are negative. A negative value of k implies a change in the direction of the x-component of the wavenumber vector. Thus the inclination of the symmetric waves with respect to the basic-state flow has changed signs. This result for the modes of maximum growth rate is analogous to that found by Busse & Chen (1981) for the marginally stable waves (see §1). Also of note is the rapid increase of k(max) for decreasing Ri.

We now turn our attention to results for $\sigma = 1.0$. What we found was unexpected. Figures 12 (*a*, *b*) summarize the results for the case $\sigma = 1.0$, $\Delta T = -0.2$ and $E = 10^{-3}$. Figure 12 (*a*) shows the variation of ω_i(max) with Ri for several values of l. The curves show several important differences from all of the previous cases for both $\sigma > 1$ and $\sigma < 1$. Note first, for the range of values of Ri examined, that there does not exist

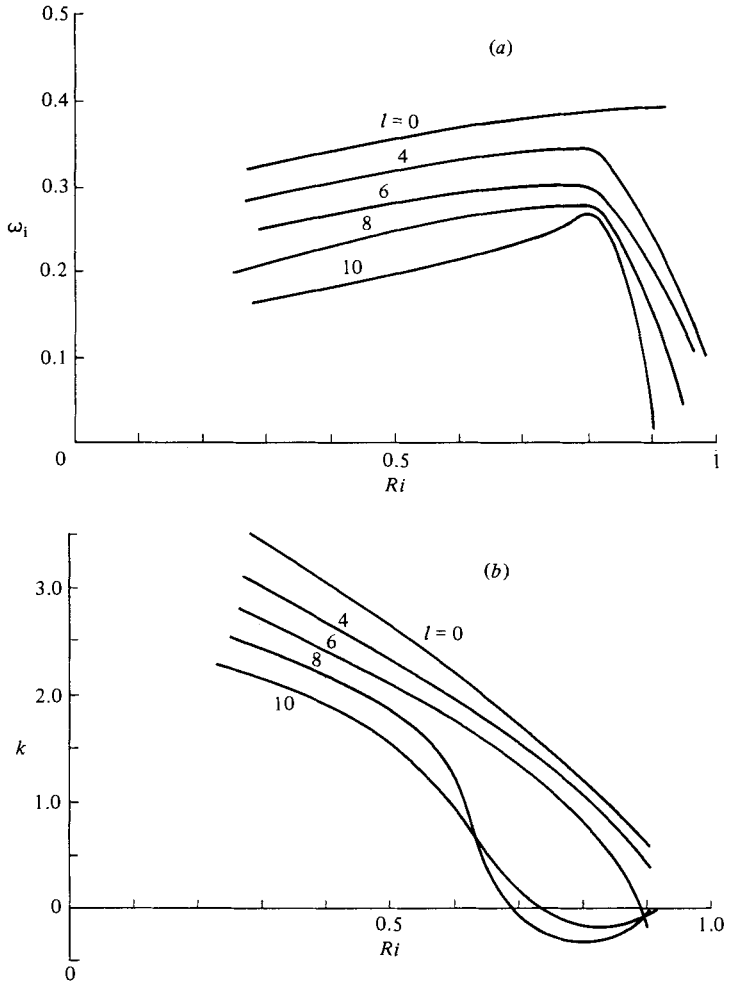

FIGURE 12. (*a*) The maximum values of ω_i as a function of Ri for $\sigma = 1.0$, $\Delta T = -0.2$, $E = 10^{-3}$ and several values of l. (*b*) The values of k at maximum ω_i as a function of Ri for the conditions of (*a*).

a value of Ri at which the transition from zonal to symmetric instability occurs. The zonal mode of maximum growth rate for $Ri > 0.9$ continues to be the preferred mode as Ri is decreased. Note also that the values of $\omega_i(\max)$ show a monotonic decrease as Ri is decreased below 0.8. Note further that the values of $\omega_i(\max)$ decrease with increasing l throughout the range shown. Another difference is that most of the ω_i versus k curves for different values of l and for specific values of Ri (not shown) show two local maxima, one in the positive range of k and the other in the negative range. (In plotting figure 12 (*a*) we used the maximum values of $\omega_i(\max)$.) This result is shown in figure 12 (*b*), which shows the variation of $k(\max)$ with Ri for several values of l. Note for the smaller wavelengths of the symmetric modes and for the larger values of Ri that the growth-rate maxima shift from negative to positive values of k as Ri is decreased. Busse & Chen (1981) predicted, for $\sigma = 1$ and for marginally stable waves and small k, that the first-order correction to the value of Ri_c is zero, indicating that the angle of inclination of the waves with respect to the basic-state flow is zero to that order. We have found from further calculations for $Ri = 0.5$, whose

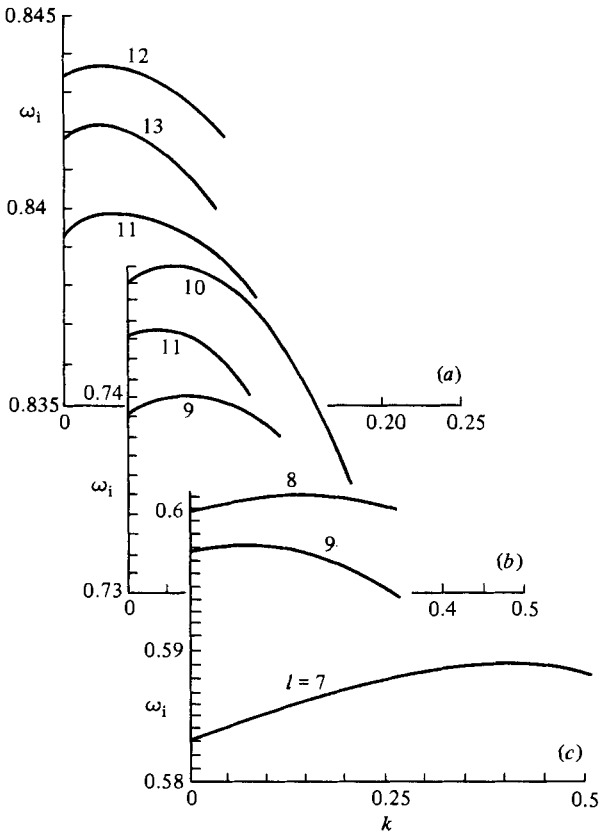

FIGURE 13. The growth rates ω_i as a function of k for $\sigma = 2$, $\Delta T = -1.5$ and $Ri = 0.5$ for (*a*) $E = 5 \times 10^{-4}$, (*b*) 10^{-3}, (*c*) 2×10^{-3}.

results are not presented here, that k for the most unstable symmetric mode is very close to zero for $\sigma = 1.1$. Clearly this result cannot be taken as a general conclusion on the value of σ at which the transition from positive to negative k occurs. It is obvious that this value of σ is a complicated function of at least Ri and E. However, a comprehensive study of this dependence is beyond the scope of the present study. On the other hand, based on our experience with this case and from the analytical work of Busse & Chen, we definitely expect this value of the transition Prandtl number to be in general very close to unity.

To investigate further the effects of viscous dissipation on symmetric baroclinic instability, we now present results for different values of the Ekman number. Figure 13 shows the growth rates of the most-unstable waves as a function of k for $E = 5 \times 10^{-4}$, 10^{-3} and 2×10^{-3} and for $\sigma = 2.0$, $\Delta T = -1.5$ and $Ri = 0.5$. The results show, for increasing E, that the growth rates decrease and that the meridional wavelengths increase. Both of these results are what we would expect, in general, when the effects of viscous dissipation are increased. This effect can also be seen in figure 8 for the pure symmetric modes for two values of the Richardson number. The results in figure 13 also show that the magnitude of the x-component of the most unstable wavenumber vector decreases with decreasing E. However, the direction of tilt (the sign of k) does not change with E. The results suggest, for the most-unstable modes, that $k \to 0$ as $E \to 0$.

Since the results for $\sigma = 1$ and $E = 10^{-3}$ (see figure 12) showed substantial differ-

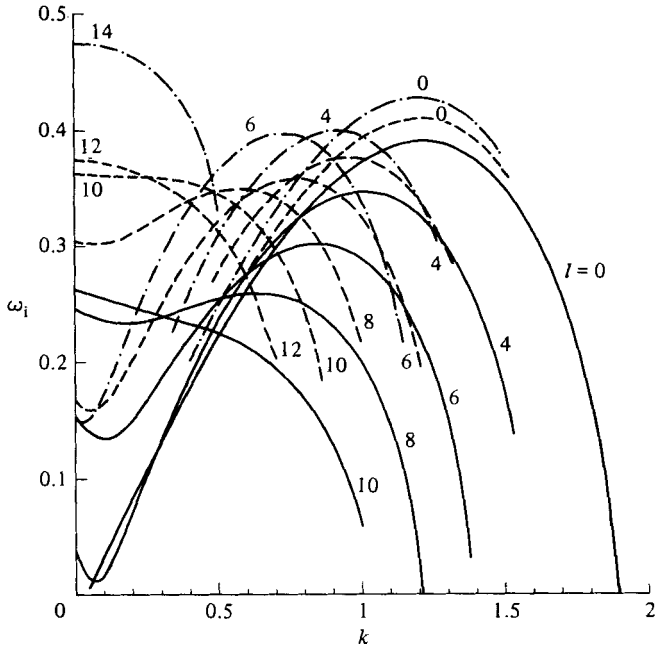

FIGURE 14. The growth rates ω_i as a function of k for $\sigma = 1$, $\Delta T = -0.2$, $Ri = 0.8$ for $E = 10^{-3}$ (——), 5×10^{-4} (– – – –), 2×10^{-4} (– · – · – · – · –).

ences from the results of other values of σ for $E = 10^{-3}$, we decided to acquire more results for $\sigma = 1$ over an extended range of E. Figure 14 shows growth rates of several meridional waves as function of k for $E = 10^{-3}$, 5×10^{-4} and 2×10^{-4} for $\sigma = 1.0$, $\Delta T = -0.2$ and $Ri = 0.8$. This value of Ri was chosen since, as shown in figure 12 (a), it is the value at which the largest $\omega_i(\max)$ occurs. The results show that for $E = 10^{-3}$ and 5×10^{-4} the regular baroclinic waves ($l = 0$) possess the maximum growth rates and hence dominate. However, as E is decreased to $E = 2 \times 10^{-4}$, the symmetric modes begin to possess the largest growth rates and hence dominate. This result is significant in that it shows that as $E \to 0$ the surprising result of the dominance of the regular baroclinic modes is no longer true. Again as in the case of figure 13, when the symmetric modes are dominant they have smaller meridional wavelengths. These results indicate, although a definitive conclusion cannot be based on this one value of Ri, that as $E \to 0$ the inviscid results of Stone (1970) are obtained (see §1). We have not surveyed the dependence of the direction of the tilt (the sign of k) of the most-unstable waves as a function of E, but the results of figure 14 show that k is zero for the symmetric mode of largest growth rate.

Busse & Chen (1981) showed that, when zonal structure is allowed, Ri_c increases above the pure symmetric value. Their analysis was limited to small values of k, but they pointed out that owing to this effect the range of Ri for which the instability occurs may be increased significantly beyond the limits observed by McIntyre (1970). Since our numerical procedure is not limited to small k, we decided to investigate this suggestion by extending the work of Busse & Chen to larger values of k. Figure 15 shows ω_i/l as a function of Ri for several values of k for $\sigma = 2.0$, $\Delta T = -1.5$, $E = 10^{-3}$ and for $l = 6$. The choice of $l = 6$ is based on previous work (AF) which showed a maximum value of Ri_c close to this value of l. In figure 15 the value of Ri_c for a specific value of k is the value of Ri at which the growth-rate curve intercepts the Ri-axis. Figure 16 shows Ri_c versus k for two values of l. For both $l = 4$ and 6

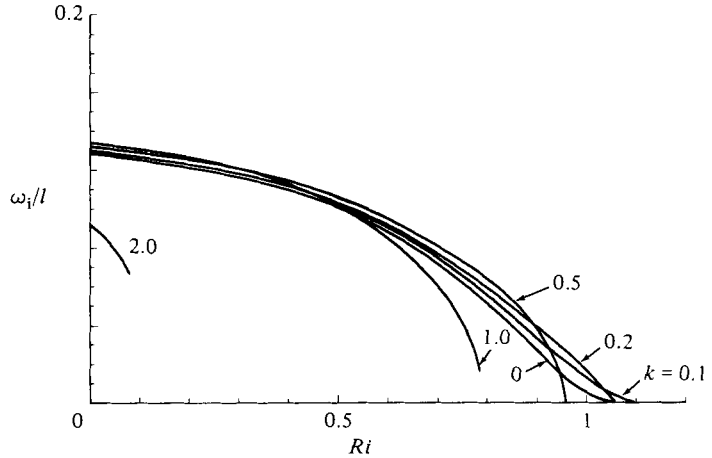

FIGURE 15. The normalized growth rate as a function of Ri for $l = 6$, $\sigma = 2.0$, $\Delta T = -1.5$, $E = 10^{-3}$ and selected values of k.

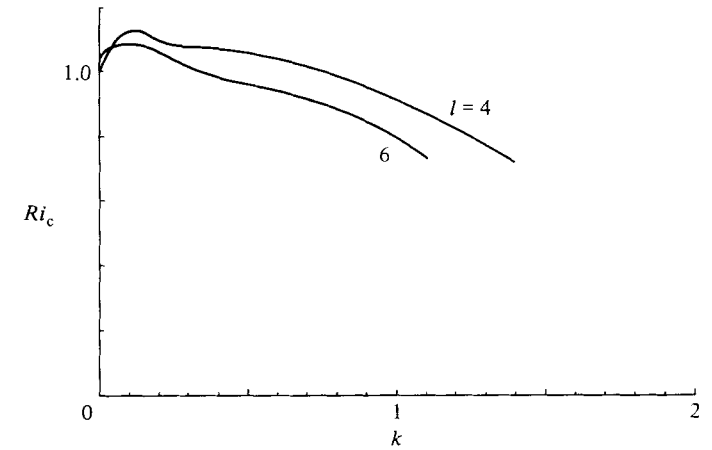

FIGURE 16. The critical Richardson number Ri_c as a function of k for $l = 4$ and 6, $\sigma = 2$, $\Delta T = -1.5$, and $E = 10^{-3}$.

the qualitative functional behaviour of Ri_c with k is similar. At first Ri_c increases with increasing k and rises above its value for $k = 0$. However, for still relatively small values of k, Ri_c reaches a maximum value which is only about 10 % greater than its value at $k = 0$, and then Ri_c declines monotonically as k increases further. Thus, we have shown, for the parameters of this computation, that the range of symmetric baroclinic instability is increased but not by much when zonal structure is permitted.

4. Conclusions

In this work we have been concerned with the three-dimensional baroclinic instability problem for $Ri = O(1)$. We have extended the inviscid analyses of Stone (1966, 1970, 1971) by adding viscous and thermal diffusion effects to the basic state and to the stability analysis and by satisfying realistic boundary conditions. Stone pointed to Ri as the significant parameter and calculated the values of Ri at which the transition between the conventional baroclinic instability, symmetric baroclinic

instability, and the Kelvin–Helmholtz instability occur (see §1). This study covers the ranges $0.135 \leqslant Ri \leqslant 1.1$, $0.2 \leqslant \sigma \leqslant 5.0$ and $2 \times 10^{-4} \leqslant E \leqslant 2 \times 10^{-3}$. We found the same general trend as Stone, namely the dominance of symmetric baroclinic instability over zonal baroclinic instability except for $\sigma = 1$ and $E \geqslant 5 \times 10^{-4}$. We found for $\sigma \neq 1$ that zonal instability dominates for $Ri > 0.825$ and symmetric instability dominates for $Ri < 0.675$. For $\sigma = 1$ and $E \geqslant 5 \times 10^{-4}$ in the range $0.3 < Ri < 0.9$, zonal instability is always preferred. However, for $\sigma = 1$ and $E = 2 \times 10^{-4}$, symmetric modes with short wavelength dominate.

We found further that the growth-rate maxima of the symmetric modes occur for waves with weak zonal structure. This means that the wavefronts are inclined at a small angle to the basic-state eastward flow (x-direction) and that the wavenumber vector is inclined at the same angle to the north (y-direction). For $\sigma > 1.1$ and $Ri = 0.5$, and $E = 10^{-3}$, the wavevector has a component towards the east and for $\sigma < 1.1$ a component towards the west.

Stone (1970) found for his inviscid model that the preferred symmetric mode is pure symmetric. Our results for finite E indicate that the zonal structure of the preferred symmetric mode becomes progressively weaker as E approaches zero.

Busse & Chen (1981) found, in the limit of small E and for small k, that the mode of symmetric instability at maximum Ri_c has weak zonal structure and hence is inclined at a small angle to the direction of the basic-state flow. This result is analogous to what we found for the preferred symmetric modes. Busse & Chen also found that Ri_c is increased over its value for $k = 0$ and they speculated that for larger k a substantial increase in the range of instability may be obtained. Our results, which are valid over a wider range of k, show that this is not so; only a small increase in Ri_c occurs at small k. Our results show that for values of Ri close to the values of Ri_c for symmetric instability, the zonal instability has much larger growth rates and hence will dominate. This result reduces the significance of previous discussions on the importance of Ri_c.

We have shown that the nearly symmetric modes of maximum growth rate differ very slightly from the pure symmetric modes. For this reason it is unlikely that they represent a new type of instability.

Let us now consider the energetics of symmetric baroclinic instability. The energy sources can be thermal or inertial or a combination of the two. For thermally driven flows potential energy is the ultimate energy source in all cases. Busse & Chen (1981) commented on the energetics of the preferred symmetric baroclinic modes with weak zonal structure. With their limited asymptotic analysis, they showed that the inclusion of a finite non-zero value for k leads to an additional y-component of the perturbation velocity when $\sigma \neq 1$. They argued that this additional flow enables the perturbations to draw more energy from the basic state. When $\sigma > 1$ the additional source is the potential energy of the basic state, and when $\sigma < 1$ it is the kinetic energy of the basic state. Generally speaking, a finite value of k allows the disturbance motion to be more perpendicular to the mean flow.

The results of our growth-rate calculations for non-marginal, weak azimuthal waves for $\sigma \neq 1$ (or more accurately 1.1) are consistent with the above arguments. Also the analysis of Busse & Chen depends on the fact that, as $E \to 0$, the value of $k \to 0$. Again our results for less restricted waves show this trend.

Our results for the case $\sigma = 1$ show that the inclusion of finite k at moderate values of E does not alter the dominance of conventional baroclinic instability. It appears that this result is due to the absence of double-diffusive effects at $\sigma = 1$.

It is of value to ask what the new results obtained in this study tell us about the

possibility of realizing symmetric baroclinic instability in the laboratory. Our model is physically realistic in that the full set of governing equations, including viscous and thermal diffusion, was used and in that realistic boundary conditions on the horizontal surfaces were satisfied. The model departs from laboratory reality in that a linear stability analysis rather than a nonlinear analysis was performed. Further, a horizontally infinite layer is, of course, unrealizable, but a shallow and wide cylindrical annulus of fluid can be realized. Although the results of § 3 indicate that the preferred mode of symmetric instability occurs with a large zonal wavelength and is not purely symmetric, this may not be so in finite cylindrical geometry when the azimuthal wavelength exceeds the circumference. We have constructed an apparatus in which a shallow layer of liquid is held between two horizontally mounted disks. Radial temperature gradients with different imposed vertical temperature differences can be maintained on the disks. The disks are made of sapphire material, their transparency allowing observation of the liquid. Sapphire is also a good thermal conductor allowing for accurate temperature boundary conditions. The total apparatus is rotated on a turntable. We have started a systematic search within the parameter ranges of the theoretical work presented in this paper, in particular $0 < Ri < 1$, and are looking for convective rolls with radial structure and weak or no azimuthal structure.

All of the computations reported in this paper were performed at the University of Tennessee computing centre. Knoxville, whose generosity is greatly appreciated. Partial funding for these computations was provided by the University of Tennessee Space Institute. Basil N. Antar wishes to acknowledge receipt of contract NAS8-33386 from NASA/Marshall Space Flight Center which he held during the performance of this investigation. This research was supported by the Global-Scale Atmospheric Processes Research Program of the Office of Science and Applications, NASA Headquarters, Washington, D.C.

REFERENCES

ANTAR, B. N. & FOWLIS, W. W. 1981 Baroclinic instability of a rotating Hadley cell. *J. Atmos. Sci.* **38**, 2130–2141.

ANTAR, B. N. & FOWLIS, W. W. 1982 Symmetric baroclinic instability of a Hadley cell. *J. Atmos. Sci.* **39**, 1280–1289.

BENNETS, D. A. & HOSKINS, B. J. 1979 Conditional symmetric instability a possible explanation for frontal rainbands. *Q. J. R. Met. Soc.* **105**, 945–962.

BUSSE, F. H. & CHEN, W. L. 1981 On the (nearly) symmetric instability. *J. Atmos. Sci.* **38**, 877–880.

CALMAN, J. 1977 Experiments on high Richardson number instability of a rotating stratified shear flow. *Dyn. Atmos. Oceans* **1**, 277–297.

CHARNEY, J. G. 1947 The dynamics of long waves in a baroclinic westerly current. *J. Met.* **4**, 135–162.

CONTE, S. D. 1966 The numerical solution of linear boundary value problems. *S.I.A.M. Rev.* **8**, 309–320.

EADY, E. T. 1949 Long waves and cyclone waves. *Tellus* **1**, 35–52.

EMANUEL, K. A. 1979 Inertial instability and mesoscale convective systems. Part I: Linear theory of inertial instability in rotating viscous fluids. *J. Atmos. Sci.* **36**, 2425–2449.

HADLOCK, R. K., NA, J. Y. & STONE, P. H. 1972 Direct thermal verification of symmetric baroclinic instability. *J. Atmos. Sci.* **29**, 1391–1393.

HIDE, R. & MASON, P. J. 1975 Sloping convection in a rotating fluid. *Adv. Phys.* **24**, 47–100.

KUO, H. L. 1956 Forced and free axially symmetric convection produced by differential heating in a rotating fluid. *J. Met.* **13**, 521–527.

LORENZ, E. N. 1967 *The Nature and Theory of the General Circulation of the Atmosphere.* World Meteorological Organization.

MCINTYRE, M. E. 1970 Diffusive destabilization of the baroclinic circular vortex. *Geophys. Fluid Dyn.* **1**, 19–57.

PEDLOSKY, J. 1979 *Geophysical Fluid Dynamics.* Springer.

SOLBERG, H. 1936 *Le Mouvement d'inertie de l'atmosphère stable et son rôle dans le théorie des cyclones.* In *Proc. Union Géodesique et Géophysique Internationale VIième Assemblée, Edinburgh*, vol. II, pp. 66–82.

STONE, P. H. 1966 On non-geostrophic baroclinic stability. *J. Atmos. Sci.* **23**, 390–400.

STONE, P. H. 1967 An application of baroclinic stability theory to the dynamics of the Jovian atmosphere. *J. Atmos. Sci.* **24**, 642–652.

STONE, P. H. 1970 On non-geostrophic baroclinic stability: Part II. *J. Atmos. Sci.* **27**, 721–726.

STONE, P. H. 1971 Baroclinic stability under non-hydrostatic conditions. *J. Fluid Mech.* **45**, 659–671.

STONE, P. H., HESS, S., HADLOCK, R. & RAY, P. 1969 Preliminary results of experiments with symmetric baroclinic instability. *J. Atmos. Sci.* **26**, 991–996.

TOKIOKA, T. 1970 Non-geostrophic and non-hydrostatic stability of a baroclinic fluid. *J. Met. Soc. Japan* **48**, 503–520.